

Journal of Biomedical Optics

BiomedicalOptics.SPIEDigitalLibrary.org

Tracking delivery of a drug surrogate in the porcine heart using photoacoustic imaging and spectroscopy

Kenneth J. Furdella
Russell S. Witte
Jonathan P. Vande Geest

SPIE.

Kenneth J. Furdella, Russell S. Witte, Jonathan P. Vande Geest, "Tracking delivery of a drug surrogate in the porcine heart using photoacoustic imaging and spectroscopy," *J. Biomed. Opt.* **22**(4), 041016 (2017), doi: 10.1117/1.JBO.22.4.041016.

Tracking delivery of a drug surrogate in the porcine heart using photoacoustic imaging and spectroscopy

Kenneth J. Furdella,^{a,†} Russell S. Witte,^{b,†} and Jonathan P. Vande Geest^{a,*}

^aUniversity of Pittsburgh, Department of Bioengineering, Pittsburgh, Pennsylvania, United States

^bUniversity of Arizona, Department of Medical Imaging, Tucson, Arizona, United States

Abstract. Although the drug-eluting stent (DES) has dramatically reduced the rate of coronary restenosis, it still occurs in up to 20% of patients with a DES. Monitoring drug delivery could be one way to decrease restenosis rates. We demonstrate real-time photoacoustic imaging and spectroscopy (PAIS) using a wavelength-tunable visible laser and clinical ultrasound scanner to track cardiac drug delivery. The photoacoustic signal was initially calibrated using porcine myocardial samples soaked with a known concentration of a drug surrogate (Dil). Next, an *in situ* coronary artery was perfused with Dil for 20 min and imaged to monitor dye transport in the tissue. Finally, a partially Dil-coated stent was inserted into the porcine brachiocephalic trunk for imaging. The photoacoustic signal was proportional to the Dil concentration between 2.4 and 120 $\mu\text{g/ml}$, and the dye was detected over 1.5 mm from the targeted coronary vessel. Photoacoustic imaging was also able to differentiate the Dil-coated portion of the stent from the uncoated region. These results suggest that PAIS can track drug delivery to cardiac tissue and detect drugs loaded onto a stent with sub-mm precision. Future work using PAIS may help improve DES design and reduce the probability of restenosis. © 2017 Society of Photo-Optical Instrumentation Engineers (SPIE) [DOI: 10.1117/1.JBO.22.4.041016]

Keywords: photoacoustic imaging; coronary heart disease; left anterior descending coronary artery; tracking diffusion; drug-eluting stent; ultrasound imaging; spectroscopy; intravascular ultrasound.

Paper 160638SSRR received Sep. 15, 2016; accepted for publication Jan. 20, 2017; published online Feb. 13, 2017.

1 Introduction

Percutaneous coronary intervention is performed in almost 0.5 million cases each year in the United States and involves placement of a stent with a balloon that is inflated in the diseased coronary artery.¹ This procedure has improved in recent years with the advent of the drug-eluting stent (DES). There is still concern about failure rates from vessel renarrowing, restenosis, with cases occurring in up to 20% of patients.¹⁻⁵ We hypothesize that these failures would be minimized by evaluating *in situ* coronary artery drug delivery.⁶⁻¹⁴

Restenosis was minimized by improving drug retention and transport in the coronary artery. Drug delivery to the tunica media has reduced or prevented migration and proliferation of vascular smooth muscle cells that cause restenosis.¹⁵ Drug diffusion and retention has also increased by modifying the drug's physiochemical properties. For example, the 42' hydroxyl group on rapamycin (a common drug on DES) has been replaced with a tetrazole ring (zotarolimus) that improves hydrophobicity, promoting retention and prolonged release, while minimizing washout.^{14,16}

The design and performance of a DES may be enhanced by monitoring or visualizing drug delivery to the coronary artery. This is supported by our findings that demonstrate drug transport and mechanical properties of the porcine coronary arteries vary as a function of vessel and location.⁶⁻⁸ However, currently, there is no ideal imaging modality to monitor and quantify drug delivery to the coronary artery with sub-mm precision.

Although noninvasive imaging modalities, such as magnetic resonance imaging, computed tomography, and ultrasound (US), are capable of anatomical and functional imaging of the heart and coronary artery, they typically lack sufficient contrast to identify and track pharmacologic compounds in the vasculature and myocardium. Optical imaging techniques have drawbacks as well. Fluorescence microscopy and histology require toxic dyes and tissue destruction. Multiphoton confocal microscopy has limited depth penetration of less than 1 mm.^{6,17,18} As a result, there are drawbacks to popular techniques used for tracking drug delivery from a DES in an intact heart. On the other hand, photoacoustic (PA) imaging and spectroscopy combined with pulse echo (PE) US potentially overcomes these limitations by offering real-time volumetric imaging with sub-mm resolution deep into tissue. With the benefit of spectroscopy, photoacoustic imaging and spectroscopy (PAIS) also provides high contrast and specificity for detecting and tracking optically absorbing compounds in the vascular tissue and myocardium. These attributes are not only favorable for testing and improving the performance of a DES, but the technology is potentially translatable for *in vivo* imaging in large animals and humans.

PA imaging is based on the PA effect, the generation of acoustic waves caused by the absorption of a short pulse of light, transient heating, and thermoelastic expansion. These acoustic waves are detected to form an US image with contrast proportional to the absorption of light, which depends on the optical wavelength. The distribution and relative concentration of optically absorbing drugs and contrast agents can also be estimated with high specificity by sweeping the optical wavelengths. In this study, we

*Address all correspondence to: Jonathan P. Vande Geest, E-mail: jpv20@pitt.edu

[†]Authors contributed equally

propose PAIS as a method to track transport of a drug surrogate in the porcine myocardium and coronary arteries. We also demonstrate imaging of a laser-sintered DES coated with a drug surrogate (also a PA contrast agent) and track its position in the intact porcine brachiocephalic trunk.

2 Materials and Methods

Optical and US setup: a wavelength-tunable laser (Surelite-II OPO, Continuum, 5-ns pulses, 20-Hz pulse repetition rate, and 20 mJ/pulse) operating between 410 and 670 nm was coupled into a 1.6-mm-diameter multimode optical fiber (CeramOptec) that connected to a “photoacoustic enabling device” (PED). Specifically, the PED held both the optical components and linear US array (Zonare L10-5, 7.1-MHz center frequency, and 5-MHz bandwidth) for coregistered PE and PA imaging, which has been previously described.^{19,20} Furthermore, the PED allowed for coalignment between the optical illumination and plane of US detection. Briefly, light from the fiber passed through a cylindrical lens to provide line illumination at the surface of the tissue. The backscattered PA waves were reflected by an inline acoustic reflector before being detected by the linear array and recorded in real-time by a clinical US scanner (zOneUltra, Zonare Medical Systems). The PED was filled with water for acoustic coupling. Raw frame data (amplitude and phase) were transferred from the scanner to a personal computer running MATLAB™ for sum-delay beamforming and postsignal processing. The axial and lateral resolutions of the PA imaging system were 300 and 400 μm , respectively.¹⁹ The slice thickness was ~ 2 mm. The fluence on the surface of the heart was ~ 10 mJ/cm² and below the American National Standards Institute safety limit of 20 mJ/cm² per pulse light at visible wavelengths.²¹

Drug surrogate: 1,1'-dioctadecyl-3,3',3'-tertramethylindocarbocyanine perchlorate (DiI) was selected for PA imaging due to its weight match to rapamycin, hydrophobic nature, cost, and favorable absorbance spectrum at visible wavelengths [Fig. 1(b)].⁶ DiI was acquired from Invitrogen (Carlsbad, California).

2.1 Image Processing and PA Signal Decomposition (Unmixing)

The primary optical absorbers at visible wavelengths in this study were the myocardium and DiI, which were separated by spectral decomposition. The PA signal is calculated as

$$PA = T * \phi * \mu, \quad (1)$$

where PA is the PA signal in MPa, T is the dimensionless Grüneisen constant that converts optical energy into acoustic pressure, ϕ is the laser fluence J/cm², and μ is the total absorption coefficient in cm⁻¹.²² Total tissue absorption equals the sum of the signals obtained, which is described as

$$\mu_{\text{total}} = \sum_{m=1}^M c_m * \mu_m, \quad (2)$$

where c_m is the concentration of the m 'th absorber, μ_m is the absorption coefficient of the m 'th absorber, and M is the number of tissue absorbers. The fraction of sample absorbers is written in matrix notation as

$$A\bar{c} = \bar{b}, \quad (3)$$

with A an $M \times N$ matrix containing the absorption coefficient of M absorbers at N wavelengths. \bar{c} is a $1 \times M$ vector containing a fractional distribution of M agents. \bar{b} is a $1 \times N$ vector of a normalized PA signal over each wavelength.⁹ The least squares of the residuals is used to solve for \hat{c}

$$\hat{c} = (A^T * A)^{-1} * A^T * \bar{b}, \quad (4)$$

\hat{c} is a signal estimation of a specific absorber based on least squares. This technique separates DiI from the myocardium and other possible absorbers such as hemoglobin.

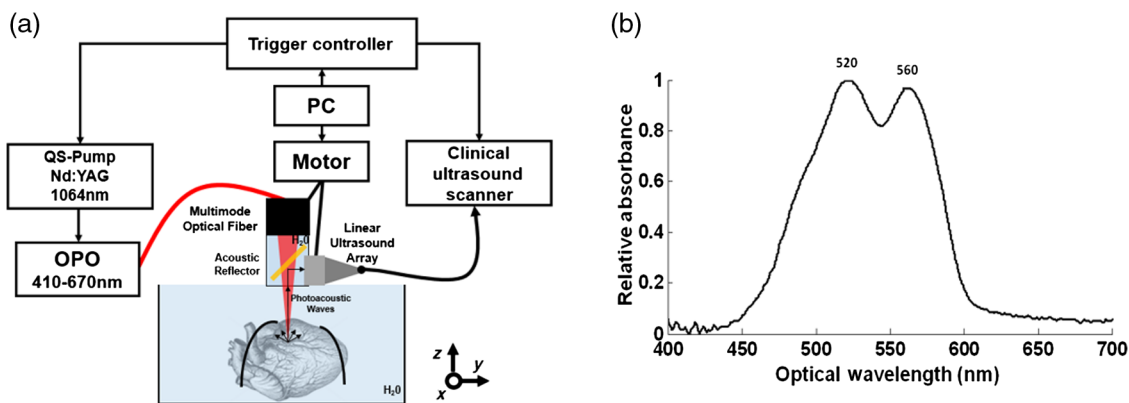


Fig. 1 PA imaging setup and optical properties of DiI. (a) Nd: YAG laser was tripled to 355 nm to pump an optical parametric oscillator and produce tunable 5 ns pulses between 410 and 670 nm. Laser light was coupled into a 1.6-mm-diameter multimode glass fiber. The fiber connected to a PA flashlight adapter, including an optical assembly with a cylindrical lens to produce a line pattern on the heart.²⁰ The adapter also contained a water-filled cavity for acoustic coupling and an acoustic reflector, which ensures coalignment of the light with the plane of US detection. A clinical US scanner (zOneUltra, Zonare Medical Systems) and 7-MHz linear array (L10-5) recorded the raw acoustic signals (phase and amplitude) for US and PA imaging. The frame data were transferred to a PC for beamforming, postprocessing, and analysis in MATLAB™. (b) Optical absorption spectrum of DiI as measured with a photospectrometer (Ocean Optics, USB4000).

2.2 Photoacoustic Imaging Experiments

2.2.1 Porcine cardiac tissue

All tissue obtained in this study was approved through the University of Arizona Institutional Animal Care and Use Committee. Adult porcine hearts ($n = 5$) were acquired from the University of Arizona Food Products and Safety Laboratory and maintained at 4°C for up to 24 h until imaging.

2.2.2 Validation and calibration in excised myocardium

A porcine left ventricle was cut into seven rectangular sections ($\sim 1 \times 1 \times 0.5$ cm). Samples were soaked in DiI for 24 h at different concentrations (0, 2.4, 4.8, 9.6, 38.4, 76.8, and 120 $\mu\text{g}/\text{ml}$) and embedded in agarose gel. Volumetric PA and US images were collected by scanning the linear array along the elevational axis with 100 μm increments. The average PA signal was calculated over the region of interest (ROI), which was determined from the coregistered B mode US image and excluded the tissue boundary. A calibration curve was generated by plotting the average PA signal versus the DiI concentration.

2.2.3 In situ porcine heart imaging

Three porcine hearts were cut proximal and distal to the coronary artery, and a cannula was inserted into the left anterior descending coronary artery (LADCA), which was initially flushed with water using a syringe pump (KD Scientific KDS230 KDS 230 Multi-Syringe Pump). Standard US helped identify the vessel location, size, and structure. Cross sectional PA images were taken from 430 to 670 nm (10 nm increments). The porcine LADCA was perfused with 2.4 $\mu\text{g}/\text{ml}$ and maintained for 20 min, followed by imaging, flushing with water, and reimaging with PE and PA. The process was repeated at incrementally higher concentrations (i.e., 12 and 60 $\mu\text{g}/\text{ml}$). The relative contribution of DiI at each pixel was determined from spectral decomposition. The distribution of DiI was also used to calculate coronary artery diffusion area and distance. Diffusion area was calculated by subtracting the background from the DiI signal and setting a threshold value. The total number of pixels with DiI was multiplied by the pixel size (0.05 mm \times 0.05 mm) to determine the diffusion area. The center of the LADCA was determined from the PE US image, and the diffusion distance was calculated by extending a line from the LADCA center point radially outward. Continuous pixel values along the line greater than background was used to calculate diffusion distance.

2.2.4 Imaging of DiI-coated stent

A cobalt chromium stent with a sinusoidal pattern was designed in Solidworks® and fabricated by Proto Labs®. Half of the stent was dipped into DiI/PCL (60 $\mu\text{g}/\text{ml}$ DiI and PCL) solution and dried for 20 min; this process was repeated three times. A coating of polydimethylsiloxane (PDMS) was also added to prevent short-term elution. The uncoated region served as a control to compare to the coated region. The stent was initially imaged in water and, later, inserted into the brachiocephalic trunk for both PA and PE imaging.

3 Results

3.1 Validation and Calibration in Excised Myocardium

Images of four of the seven myocardial samples are displayed in Fig. 2. Wavelengths of 550 and 660 nm represented the local maximum and minimum for DiI absorption in the visible range. Whereas at 550 nm, the PA image was dominated by DiI absorption, at 660 nm the image was dominated by the intrinsic absorption of the myocardium. In general, the PA signal intensity increased linearly with concentration. The final column represents the DiI concentration after unmixing the PA signal at all the wavelengths.

These data were used to generate a calibration curve for DiI in the excised myocardium. The average PA signal (over the ROI) was plotted against the prepared DiI concentration (Fig. 3). The axes are displayed in octaves to match the distribution of prepared DiI concentrations.

Figure 3 indicates a strong linear relationship spanning almost eight octaves between the DiI sample concentration and the amplitude of the PA signal. In addition, minute concentrations of DiI (<2.4 $\mu\text{g}/\text{ml}$) could be detected at high spatial resolution (<300 μm) deep in tissue (>5 mm). These favorable attributes of PA imaging were extended to study transport in the porcine coronary artery and myocardium.

3.2 Imaging of the Porcine Heart (In Situ)

DiI at 2.4 $\mu\text{g}/\text{ml}$ was perfused into the LADCA for 15 s (see Fig. 4). The PA signal at 550 nm near branching vessels increased linearly during the perfusion, demonstrating real-time capabilities of PA imaging for tracking drug transport and diffusion.

Estimates of DiI diffusion in the porcine heart are presented in Fig. 5. The PA spectrum was dominated by absorption of the myocardium except at regions with high DiI. Areas of DiI diffusion for 2.4, 12, and 60 $\mu\text{g}/\text{ml}$ were calculated at 1.30, 1.75, and 3.30 mm^2 , respectively. Therefore, an increase in DiI concentration led to an increase in diffusion area. These results demonstrated that PA imaging can track transport of DiI, a drug surrogate.

In addition to diffusion area, we also calculated the diffusion distance from the center of LADCA, which depended on the concentration (see Fig. 6). DiI diffused an average of 0.95 ± 0.37 mm, ranging from 0.6 to 1.5 mm [Fig. 6(c)]. These results suggest that PA imaging can track transport several millimeters from the coronary into the myocardium.

3.3 Ultrasound and Photoacoustic Imaging of a DiI-Coated Stent

A cardiovascular stent was fabricated to test if PA imaging could detect DiI coated on a stent placed inside a blood vessel. Images of the DiI-coated cardiovascular stent are presented in Fig. 7. PA imaging was able to differentiate the coated versus uncoated region in water and in the brachiocephalic trunk [Figs. 7(d) and 7(f), respectively]. These results demonstrated that PA imaging was able to detect DiI on a stent placed inside a large blood vessel.

4 Discussion

Our results demonstrated that PAIS is a nondestructive method that tracks drug delivery in the porcine vasculature while

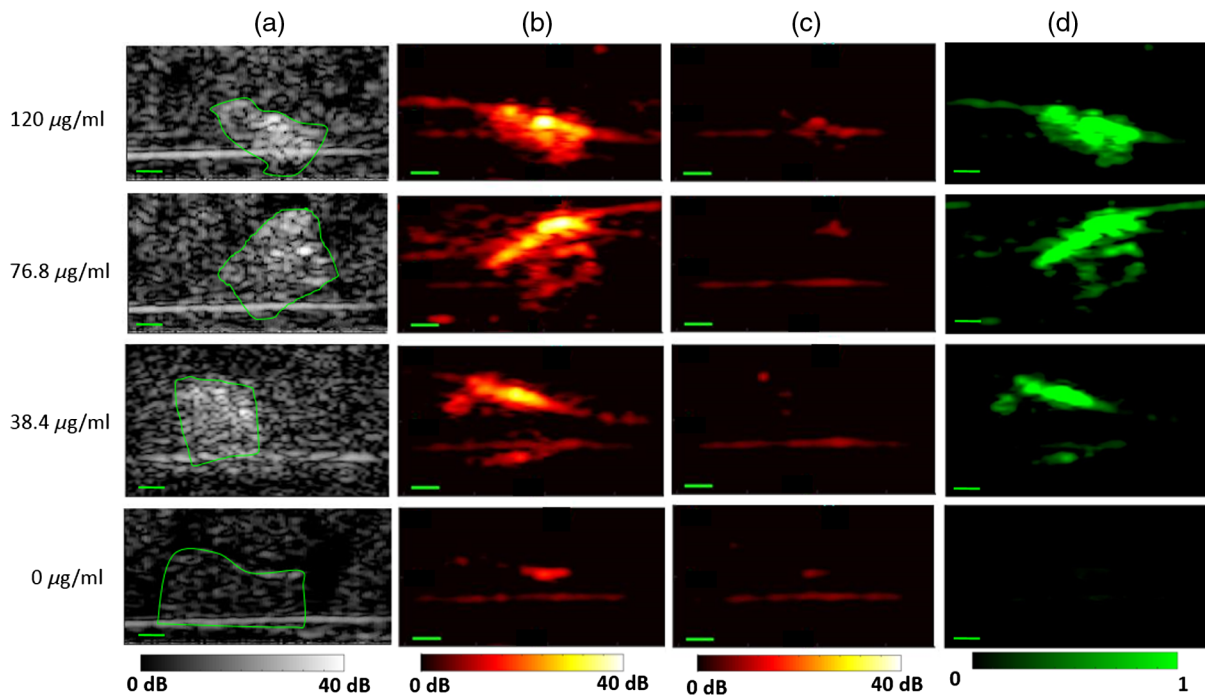


Fig. 2 US and PA imaging of porcine myocardial samples stained with Dil. Each row represents a sample stained with a different concentration of Dil (0, 38.4, 76.8, and 120 $\mu\text{g/ml}$). (a) Cross-sectional PE US images of samples embedded in Agarose™. Samples are outlined in green. (b) Corresponding PA signal at 550 nm (near peak of Dil absorption). (c) PA signal at 660 nm (low Dil absorption). (d) Relative concentration of Dil after spectral decomposition. Green scale bar represents 2 mm.

providing excellent contrast, depth, and resolution. PAIS was able to quantify the distribution of a drug surrogate at concentrations from 2.4 to 120 $\mu\text{g/ml}$. Perfusion of Dil into the coronary artery increased the PA signal in the surrounding tissue greater than 1.5 mm away from the targeted vessel. PAIS was also able to differentiate the brachiocephalic trunk from the coated and uncoated regions of a stent. Our results suggest that PAIS may be a valuable tool for tracking drug delivery to a specific vessel and provide feedback on drugs loaded onto a DES. In this regard, PAIS may help improve the design of a

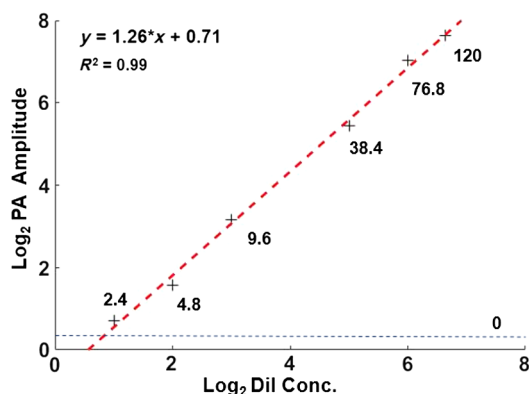


Fig. 3 PA calibration curve for Dil. The pixel values over the ROI were averaged and plotted against the prepared concentration of Dil for each sample. The equation for the best fit line (dashed red) and R^2 value are also indicated. All concentration values are in $\mu\text{g/ml}$. Based on the PA signal without Dil (blue-dashed line), the sensitivity of PA for detecting the dye in the samples was ~ 2 $\mu\text{g/ml}$.

DES, increase drug retention and delivery to the coronaries arteries, and reduce in-stent restenosis.

Our approach has not only demonstrated that PAIS may be a useful tool for assessing drug delivery *in vitro* but could also be used in preclinical animal models of vascular disease. For example, a porcine thoracic window to the coronary artery could provide time course information about *in vivo* drug delivery.²³ Specifically, DES polymer degradation and therapeutic drug transport could be monitored over time in the same animal, thus minimizing the number of animals used in preclinical studies. Our results further suggest that the PA signal from the stent and surrounding tissues could be used to estimate drug concentrations thus providing real-time feedback for improving DES designs.

To visualize drug delivery, this study implemented a drug surrogate with a peak absorption near 550 nm. At this wavelength, penetration depth in cardiac tissue is about ~ 5 mm due to overlap in intrinsic background absorption (e.g., hemoglobin). However, if the drug surrogate is exchanged for a near-infrared (NIR) absorber, PAIS should be able to track drug delivery even deeper (>10 mm) into tissue with less interference from background absorption.²³ In this case, it may be possible to use fewer wavelengths for spectral decomposition, thereby simplifying the imaging procedure and scan time. In general, most restenosis drugs absorb in the ultraviolet range, which limits penetration depth.^{24,25} Therefore, it could be desirable to conjugate a small-molecule dye onto the drug to track delivery using PAIS. For example, the 42' hydroxyl group on rapamycin has shown great promise for conjugation of an optically absorbing dye. One group has successfully attached 7-bromo-4-nitrobenzofurazan, a visible spectrum dye, onto rapamycin.²⁶ Conjugating rapamycin with a visible or NIR absorber would

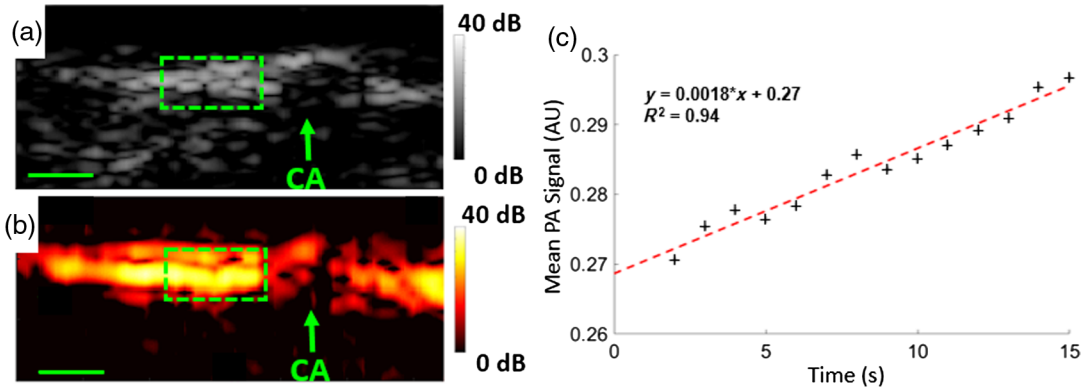


Fig. 4 Increase in PA signal near LADCA during Dil perfusion. (a) Cross sectional PE image of an *ex vivo* porcine heart. (b) Coregistered PA image at 550 nm during infusion of 2.4 $\mu\text{g/ml}$ Dil. Vessel pressure was maintained at 70 mm Hg. (c) Average PA signal over time inside dashed green box during infusion of Dil. The PA signal increase is observed in myocardial tissue adjacent to the coronary (CA) vessel. The scale bar denotes 2 mm.

facilitate PAIS for quantifying drug delivery to the coronary artery.

In order to track drug delivery, there are many confounding factors that affect the PA signal in the heart: dye concentration,

laser fluence, sample geometry, dye distribution, background absorption, and photobleaching. To reduce effects of pulse-to-pulse variations of the laser, we averaged the signal at each location over several pulses. Photobleaching of the dye

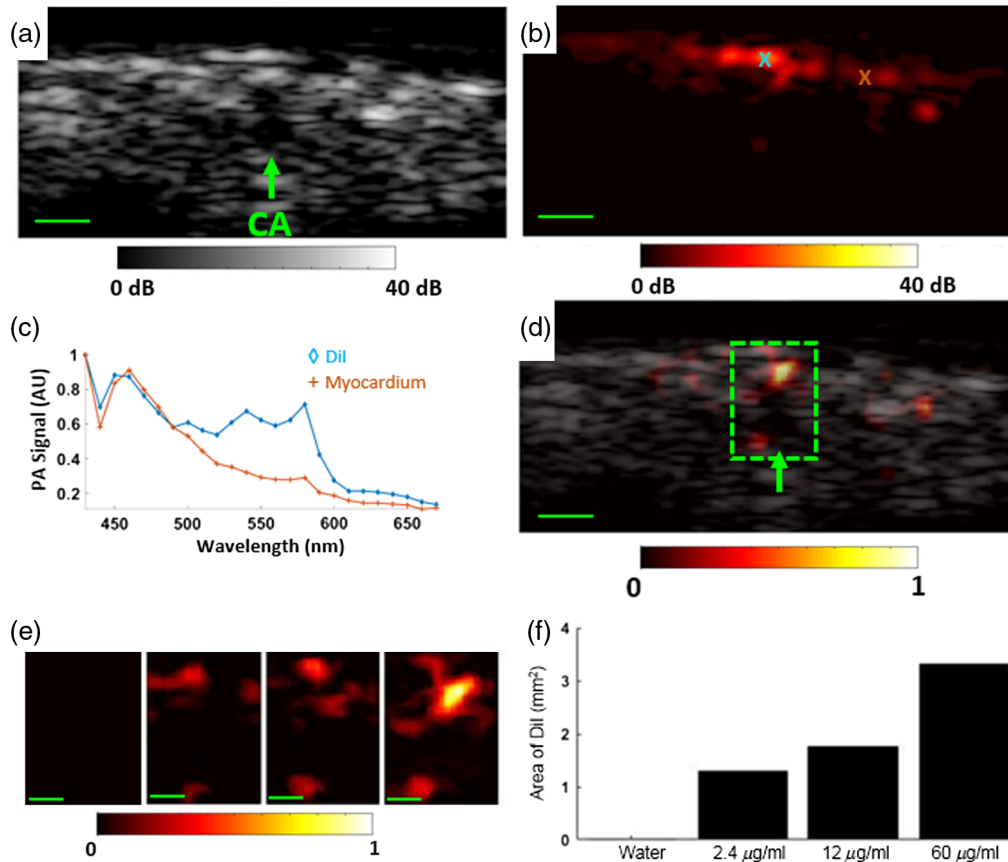


Fig. 5 Estimation of Dil diffusion in the heart near the LADCA. (a) Cross sectional PE US image over LADCA. (b) Coregistered PA image at 550 nm with a dynamic range of 40 dB. The PA spectra over regions of interest marked with "X" are displayed in (c). Brown and blue regions are similar to the known absorption spectra of the myocardium and Dil, respectively. (d) Coregistered PE (gray) and unmixed PA signal for 60 $\mu\text{g/ml}$ Dil concentration (following flush). Green box identifies the ROI for cumulative diffusion analysis. (e) PA images over ROI (green box) for Dil concentration of 0 (100% water), 2.4, 12, and 60 $\mu\text{g/ml}$. (f) Diffusion area for each concentration based on PA signal over background. Scale bar is 2 mm.

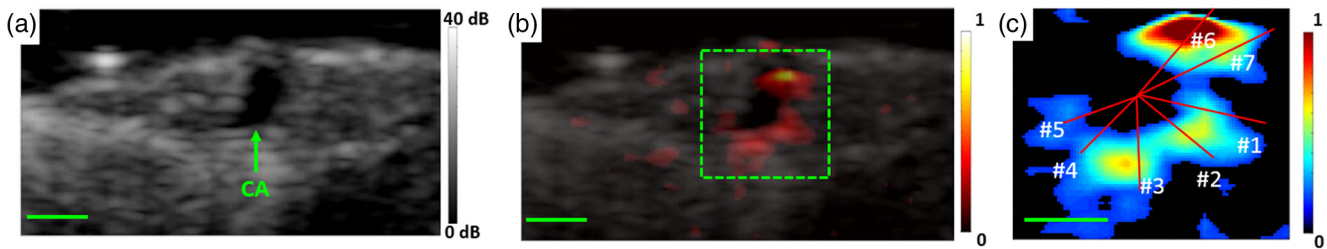


Fig. 6 Diffusion distance from LADCA. (a) Cross sectional US image of the LADCA in the porcine heart. (b) Overlay of PE US (gray) and PA (hot) images. Scale bar = 2 mm. (c) Calculation of diffusion distance from LADCA based on signal above threshold noise inside dashed box in (b). Diffusion distance for this example ranged from 0.6 to 1.5 mm. Scale bar = 1 mm.

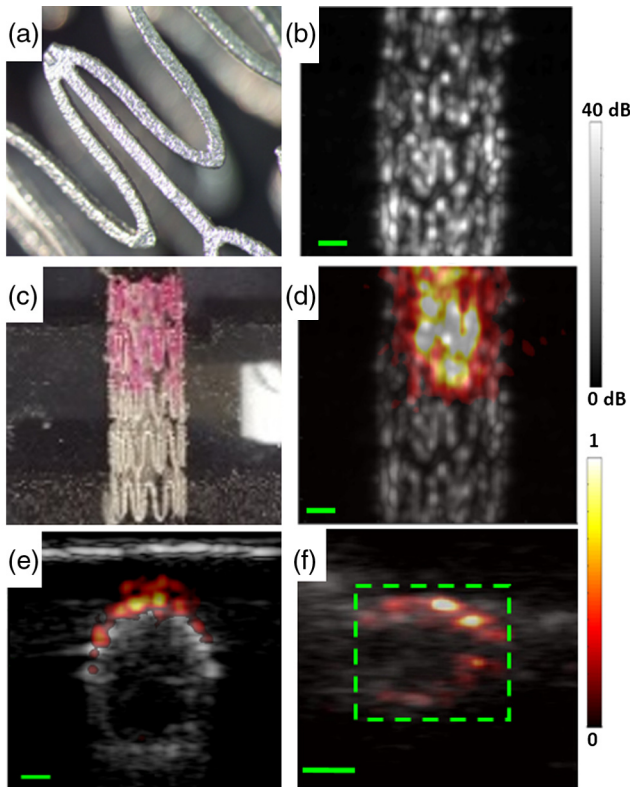


Fig. 7 PE and PA imaging of Dil-coated cardiovascular stent. (a) Zoomed-in photograph of sinusoidal pattern of stent; (b) top view PE US image of stent at 7.1 MHz. (c) Top view photograph of stent with Dil/PCL + PDMS coating on top half. (d and e) Coregistered PE US (gray) and PA (hot) at 550 nm image (d = long view, e = cross view) of stent in water with coating on top half. (f) Coregistered US and unmixed PA signal of stent implanted in the brachiocephalic trunk. Scale bar = 2 mm. Green box highlights the stent in the blood vessel.

was also kept to a minimum by only exposing the samples to light while recording data (typically less than 10 pulses at each location). To reduce effects of the geometry on the PA signal during the calibration experiment, each sample was cut to a similar size and shape and placed in the agarose gel at the same depth. The ROIs were chosen inside the sample to reduce boundary effects of the PA signal. Finally, dye variations inside each sample were reduced by soaking the samples for 24 h in the dye. A similar protocol was employed by Keyes et al. prior to PA imaging in porcine LADCA samples.⁶ In that study, it was assumed that 24 h was sufficient for saturation of the dye in the tissue.

There were two other primary limitations in this study. First, the spatial resolution of $\sim 300 \mu\text{m}$ was limited by the 5-MHz bandwidth of the US transducer. A higher frequency US probe (e.g., $>50 \text{ MHz}$) could be incorporated into our system to improve the resolution to less than $50 \mu\text{m}$, which would be sufficient to track diffusion through layers of the coronary wall.²⁷ Another limitation was the inability to directly apply our setup to image the heart *in vivo*. Although transthoracic PA imaging is possible, penetration would be limited to about 2 cm. In this case, intravascular US/PA (PA-IVUS) would be the most practical solution for *in vivo* cardiac imaging of a DES. Currently, PA-IVUS has been used to track the position of a stent and detect vulnerable plaque in animal models.^{28–31} Such probes are being developed and tested by other groups with the ultimate goal of clinical translation.^{29,32–35}

In summary, this study demonstrated that PA imaging offers excellent spatial resolution, penetration, and contrast for tracking transport of a drug surrogate in the porcine vasculature. PAIS also improves the specificity for estimating drug concentrations by separating the signal from intrinsic background absorbers in cardiac tissue. *In vivo* PA imaging of drug retention and delivery in the coronaries could help improve the design and performance of a DES and reduce the probability of restenosis during interventional treatment of CHD.

Disclosures

No conflicts of interest, financial or otherwise, are declared by the authors.

Acknowledgments

This research was funded by the National Science Foundation GK-12 fellowship and the Technology Research Initiative Fund (TRIF). Dr. Russell S. Witte is an inventor on a patent (ultrasonic/photoacoustic imaging devices and methods, US20130039147), which has a licensing arrangement between the University of Arizona and Zonare Medical Systems.

References

1. M. Writing Group et al., "Heart disease and stroke statistics-2016 update: a report from the American Heart Association," *Circulation* **133**(4), e38–e360 (2016).
2. G. D. Dangas et al., "In-stent restenosis in the drug-eluting stent era," *J. Am. Coll. Cardiol.* **56**(23), 1897–1907 (2010).
3. J. W. Moses et al., "Sirolimus-eluting stents versus standard stents in patients with stenosis in a native coronary artery," *N. Engl. J. Med.* **349**(14), 1315–1323 (2003).
4. G. W. Stone et al., "Comparison of a polymer-based paclitaxel-eluting stent with a bare metal stent in patients with complex coronary artery

- disease: a randomized controlled trial," *J. Am. Med. Assoc.* **294**(10), 1215–1223 (2005).
5. M. C. Morice et al., "Sirolimus-vs paclitaxel-eluting stents in de novo coronary artery lesions: the REALITY trial: a randomized controlled trial," *J. Am. Med. Assoc.* **295**(8), 895–904 (2006).
 6. J. T. Keyes, B. R. Simon, and J. P. Vande Geest, "Location-dependent coronary artery diffusive and convective mass transport properties of a lipophilic drug surrogate measured using nonlinear microscopy," *Pharm. Res.* **30**(4), 1147–1160 (2013).
 7. J. T. Keyes, B. R. Simon, and J. P. Vande Geest, "A finite element study on variations in mass transport in stented porcine coronary arteries based on location in the coronary arterial tree," *J. Biomech. Eng.* **135**(6), 61008–61011 (2013).
 8. J. T. Keyes et al., "Deformationally dependent fluid transport properties of porcine coronary arteries based on location in the coronary vasculature," *J. Mech. Behav. Biomed. Mater.* **17**, 296–306 (2013).
 9. A. M. Malek, S. L. Alper, and S. Izumo, "Hemodynamic shear stress and its role in atherosclerosis," *J. Am. Med. Assoc.* **282**(21), 2035–2042 (1999).
 10. J. D. Talley et al., "Failed elective percutaneous transluminal coronary angioplasty requiring coronary artery bypass surgery. In-hospital and late clinical outcome at 5 years," *Circulation* **82**(4), 1203–1213 (1990).
 11. G. S. Roubin, S. B. King, 3rd, and J. S. Douglas Jr., "Restenosis after percutaneous transluminal coronary angioplasty: the Emory University Hospital experience," *Am. J. Cardiol.* **60**(3), 39b–43b (1987).
 12. S. L. Chen et al., "Crush stenting with drug-eluting stents: relevance of coronary bifurcation lesion location on angiographic and clinical outcomes," *Clin. Cardiol.* **33**(12), E32–E39 (2010).
 13. S. Elezi et al., "Vessel size and outcome after coronary drug-eluting stent placement: results from a large cohort of patients treated with sirolimus- or paclitaxel-eluting stents," *J. Am. Coll. Cardiol.* **48**(7), 1304–1309 (2006).
 14. J. Daemen et al., "Early and late coronary stent thrombosis of sirolimus-eluting and paclitaxel-eluting stents in routine clinical practice: data from a large two-institutional cohort study," *Lancet* **369**(9562), 667–678 (2007).
 15. A. C. Newby and A. B. Zaltsman, "Molecular mechanisms in intimal hyperplasia," *J. Pathol.* **190**(3), 300–309 (2000).
 16. C. W. Hwang, D. Wu, and E. R. Edelman, "Physiological transport forces govern drug distribution for stent-based delivery," *Circulation* **104**(5), 600–605 (2001).
 17. J. Panyam and V. Labhasetwar, "Biodegradable nanoparticles for drug and gene delivery to cells and tissue," *Adv. Drug Deliv. Rev.* **55**(3), 329–347 (2003).
 18. A. Zoumi et al., "Imaging coronary artery microstructure using second-harmonic and two-photon fluorescence microscopy," *Biophys. J.* **87**(4), 2778–2786 (2004).
 19. L. G. Montilla, R. Olafsson, and R. S. Witte, "Real-time pulse echo and photoacoustic imaging using an ultrasound array and in-line reflective illumination," *Proc. SPIE* **7564**, 75643C (2010).
 20. L. G. Montilla et al., "Real-time photoacoustic and ultrasound imaging: a simple solution for clinical ultrasound systems with linear arrays," *Phys. Med. Biol.* **58**(1), N1–N12 (2013).
 21. ANSI, *American National Standard for the Safe Use of Lasers*, ANSI Z136.1, New York: American National Standards Institute (2007).
 22. L. Wang, *Biomedical Optics: Principles and Imaging*, Vol. **362**, John Wiley & Sons, Hoboken, New Jersey (2007).
 23. J. R. Rajian, P. L. Carson, and X. Wang, "Quantitative photoacoustic measurement of tissue optical absorption spectrum aided by an optical contrast agent," *Opt. Express* **17**(6), 4879–4889 (2009).
 24. F. Streit et al., "Sensitive and specific quantification of sirolimus (rapamycin) and its metabolites in blood of kidney graft recipients by HPLC/electrospray-mass spectrometry," *Clin. Chem.* **42**(9), 1417–1425 (1996).
 25. T. A. Willey et al., "High-performance liquid chromatographic procedure for the quantitative determination of paclitaxel (Taxol) in human plasma," *J. Chromatogr.* **621**(2), 231–238 (1993).
 26. D. S. Miller, G. Fricker, and J. Drewe, "p-Glycoprotein-mediated transport of a fluorescent rapamycin derivative in renal proximal tubule," *J. Pharmacol. Exp. Ther.* **282**(1), 440–444 (1997).
 27. V. Daeichin et al., "Frequency analysis of the photoacoustic signal generated by coronary atherosclerotic plaque," *Ultrasound Med. Biol.* **42**(8), 2017–2025 (2016).
 28. J. L. Su, B. Wang, and S. Y. Emelianov, "Photoacoustic imaging of coronary artery stents," *Opt. Express* **17**(22), 19894–19901 (2009).
 29. A. B. Karpiouk et al., "Feasibility of in vivo intravascular photoacoustic imaging using integrated ultrasound and photoacoustic imaging catheter," *J. Biomed. Opt.* **17**(9), 096008 (2012).
 30. X. Bai et al., "Intravascular optical-resolution photoacoustic tomography with a 1.1 mm diameter catheter," *PLoS One* **9**(3), e92463 (2014).
 31. Y. Li et al., "High-speed intravascular spectroscopic photoacoustic imaging at 1000 A-lines per second with a 0.9-mm diameter catheter," *J. Biomed. Opt.* **20**(6), 065006 (2015).
 32. B. Wang et al., "In vivo intravascular ultrasound-guided photoacoustic imaging of lipid in plaques using an animal model of atherosclerosis," *Ultrasound Med. Biol.* **38**(12), 2098–2103 (2012).
 33. X. Li et al., "Intravascular photoacoustic imaging at 35 and 80 MHz," *J. Biomed. Opt.* **17**(10), 106005 (2012).
 34. Y. Cao et al., "High-sensitivity intravascular photoacoustic imaging of lipid-laden plaque with a collinear catheter design," *Sci. Rep.* **6**, 25236 (2016).
 35. K. Jansen et al., "Photoacoustic imaging of human coronary atherosclerosis in two spectral bands," *Photoacoustics* **2**(1), 12–20 (2014).

Kenneth J. Furdella graduated from Drexel University with a BS degree in biomedical engineering in 2012. He received his master's in biomedical engineering at the University of Arizona, Tucson, in 2016. While at the University of Arizona, he worked with Jonathan Vande Geest and Russell Witte on photoacoustic imaging. Currently, he is a graduate student in bioengineering at the University of Pittsburgh. He hopes to further his research using photoacoustic imaging to track diffusion coronary arteries.

Russell S. Witte graduated with honors (BS degree in physics, 1993) from the University of Arizona and a PhD (bioengineering, 2002) from Arizona State University. As a postdoctoral fellow, he helped develop new imaging modalities for the brain, heart, and skeletal muscle. He is now associate professor of medical imaging, optical sciences, and biomedical engineering at the University of Arizona. His laboratory devises hybrid imaging and contrast mechanisms that combine light, ultrasound, and/or microwaves to address medical challenges.

Jonathan P. Vande Geest is the principal investigator of the Soft Tissue Biomechanics Laboratory (STBL) and is a professor of bioengineering at the University of Pittsburgh with affiliate faculty appointments in the McGowan Institute for Regenerative Medicine and the Vascular Medicine Institute. The STBL is focused on identifying the structure functions relationships of soft tissues in human pathophysiology using state of the art computational and experimental tools in biomechanics, imaging, and mechanobiology.